NASA TECHNICAL MEMORANDUM

NASA TM X-2975

NASA TM X-2975

DISTRIBUTED EDUCATED THROAT STABILITY BYPASS TO INCREASE THE STABLE AIRFLOW RANGE OF A MACH 2.5 INLET WITH 60-PERCENT INTERNAL CONTRACTION

by Robert J. Shaw, Glenn A. Mitchell, and Bobby W. Sanders

Lewis Research Center
Cleveland, Ohio 44135

NATIONAL AERONAUTICS AND SPACE ADMINISTRATION • WASHINGTON, D. C. • JUNE 1974

1. Report No. NASA TM X-2975	2. Government Accession No.	3. Recipient's Catalog No.
4. Title and Subtitle DISTRIBUTED EDUCATED THROAT STABILITY BYPASS TO INCREASE THE STABLE AIRFLOW RANGE OF A MACH 2.5 INLET WITH 60-PERCENT INTERNAL CONTRACTION		5. Report Date June 1974 6. Performing Organization Code
7. Author(s) Robert J. Shaw, Glenn A. Mitchell, and Bobby W. Sanders		8. Performing Organization Report No. E-7708 10. Work Unit No. 501-24
9. Performing Organization Name and Address Lewis Research Center, National Aeronautics and Space Administration, Cleveland, Ohio 44135		11. Contract or Grant No. 13. Type of Report and Period Covered Technical Memorandum
12. Sponsoring Agency Name and Address National Aeronautics and Space Administration, Washington, D.C. 20546		14. Sponsoring Agency Code
15. Supplementary Notes		

16 Abstract

The results of an experimental investigation to increase the stable airflow operating range of a supersonic mixed-compression inlet are presented. A distributed educated throat stability-bypass entrance configuration was tested. In terms of diffuser-exit corrected airflow, a large inlet stable airflow range of about 16.1 percent was obtained if a constant pressure was maintained in the bypass plenum. Limited unstart angle of attack data are presented.

17. Key Words (Suggested by Author(s))	18. Distribution Statement
Air intakes; Supersonic cruise inlets; Shock stability; Inlet bleed; Throat-bypass bleed; Throat stability bypass	Unclassified - unlimited Category 01

19. Security Classif. (of this report)	20. Security Classif. (of this page)	21. No. of Pages	22. Price*
Unclassified	Unclassified	35	$3.25

* For sale by the National Technical Information Service, Springfield, Virginia 22151

DISTRIBUTED EDUCATED THROAT STABILITY BYPASS TO INCREASE THE STABLE AIRFLOW RANGE OF A MACH 2.5 INLET WITH 60-PERCENT INTERNAL CONTRACTION

by Robert J. Shaw, Glenn A. Mitchell, and Bobby W. Sanders

Lewis Research Center

SUMMARY

An experimental investigation was conducted to evaluate the effectiveness of a distributed educated, throat stability-bypass entrance configuration in providing an increased inlet stable airflow operating range. The inlet used for this study was an axisymmetric, mixed-compression type with 60 percent of the supersonic area contraction occurring internally at the design Mach number of 2.50.

The distributed educated configuration provided the inlet with a large stability range when operating at high-performance conditions. In terms of diffuser-exit corrected airflow, such an inlet configuration could accept about a 16.1-percent reduction before unstart if a constant pressure is maintained in the bypass plenum.

With no stability bypass flow, the inlet's angle-of-attack tolerance was commensurate with results of previous tests on the same inlet model with only performance-bleed capabilities. Angle-of-attack unstarts were caused by an overcompression of the diffuser flow field on the leeward side with resulting local flow choking.

INTRODUCTION

At flight speeds above Mach 2.0 an inlet having a mixture of internal and external compression offers high performance by supplying the engine with airflow at a high-pressure level while maintaining low drag. To provide optimum internal performance for this type of inlet, the terminal shock must be kept at the inlet throat. However, mixed-compression inlets suffer from an undesirable airflow characteristic known as unstart. The closer the terminal shock to the throat, the smaller the disturbance that will cause an unstart. This airflow disturbance causes the terminal shock to move forward of the throat where it is unstable and is violently expelled ahead of the inlet cowl-

ing. This shock expulsion or unstart causes a large rapid variation in mass flow and pressure recovery, and thus a large thrust loss and drag increase. Inlet buzz, compressor stall, and/or combustor blowout may also occur. Obviously, an inlet unstart is extremely undesirable, not only because of the effects on the propulsion system itself, but also on the aerodynamic qualities of the aircraft. If an inlet unstart does occur, large variations of the inlet geometry are required to reestablish initial design operating conditions.

Both external airflow transients such as atmospheric turbulence and internal airflow changes such as a reduction in engine airflow demand can cause the inlet to unstart. It is desirable for the inlet to have a large enough stable margin to absorb such transients without unstarting. For an internal airflow change, the inlet should provide a margin in corrected airflow below the value for optimum performance without incurring unstart. This margin is defined as the stable airflow operating range. Conventional mixed-compression inlets can be designed to have some stable range provided by the capacity of the performance-bleed systems. Since performance-bleed exit areas are generally fixed, this stable range may not be adequate to absorb many of the airflow transients that are encountered by a typical supersonic propulsion system. An increased stable range may be provided by operating supercritically, with a resultant loss in performance. Since any loss in performance is reflected directly as a loss in thrust, supercritical operation should be avoided.

To provide the necessary stable operating range without compromising steady-state performance, the inlet can be designed to replace the throat bleed with a throat stability-bypass system capable of removing large amounts of airflow when needed. This system prevents unstarts by increasing bypass airflow to compensate for reductions in the diffuser-exit airflow demand. References 1 to 4 indicate that large increases in the stability-bypass airflow may be provided without prohibitive amounts of airflow removal during normal operation; that is, the exit area is controlled to maintain a relatively constant pressure in the stability-bypass plenum. This exit-area variation might either be provided by an active control using shock position sensors or by a passive control using pressure-activated valves at the stability-bypass exit. These pressure-activated valves open in response to the pressure rise in the stability-bypass plenum caused by the forward moving terminal shock. To be most effective, the valves should be designed to maintain a nearly constant stability-bypass plenum pressure. Using a Mach 2.5, mixed-compression inlet with 40-percent internal contraction, reference 2 reported that several types of stability-bypass entrance configurations were capable of producing a large stable airflow range if a constant-pressure stability-bypass exit control could be used. When these entrance configurations were used with pressure-activated valves (see refs. 3 and 4), the diffuser-exit airflow could be reduced as much as 28 percent from the optimum performance point without causing inlet unstart.

Experimental tests were conducted in the Lewis 10- by 10-Foot Supersonic Wind Tunnel to continue the evaluation of stability-bypass systems. The same types of stability-bypass systems as used in references 2 to 4 were investigated using an axisymmetric, Mach 2.5, mixed-compression inlet having 60 percent of the design supersonic area contraction occurring internally. Stability-bypass airflow was removed from the cowl side of the inlet throat region through several different entrance configurations. These entrance configurations used either a distributed porous surface, distributed educated slots, or a forward-slanted slot. The purpose of this report is to present the performance of the distributed educated entrance configuration in handling internal disturbances and to determine its suitability for use with pressure-activated valves designed to have a nearly constant pressure characteristic. The performance of the distributed porous and forward-slanted slot configurations are reported in references 5 and 6, respectively. For the data reported herein, remotely variable choked-exit plug assemblies were used to vary the stability-bypass flow.

Data were obtained at a free-stream Mach number of 2.50 and at a Reynolds number, based on inlet cowl lip diameter, of 3.88×10^6. Some data were obtained at the maximum angle of attack before unstart.

U.S. customary units were used in the design of the test model and for recording and computing of experimental data. These units were converted to the International System of Units for presentation in this report.

SYMBOLS

A	flow area, m^2
A_c	cowl lip capture area, 0.1758 m^2
AI	airflow index, $AI = 100\left\{1 - \left[(W\sqrt{\theta}/\delta)_{min\ s}/(W\sqrt{\theta}/\delta)_{op}\right]\right\}_5$, percent
D_5	steady state distortion, $\left[(P_{max} - P_{min})/P_{av}\right]_5$
d	distance from local surface, cm
H	annulus or rake height, cm
M	Mach number
m/m_0	mass-flow ratio
P	total pressure, N/m^2
p	static pressure, N/m^2
R_c	inlet cowl lip radius, 23.66 cm

r	radius, cm
SI_{cp}	constant pressure stability index, $SI_{cp} = 100\left\{1 - \left[(W\sqrt{\theta}/\delta)_{\text{min s, cp}}/(W\sqrt{\theta}/\delta)_{op}\right]_5\right\}$, percent
T	total temperature, K
W	airflow, kg/sec
$W\sqrt{\theta}/\delta$	corrected airflow, kg/sec
x	axial distance from cone tip, cm
α	angle of attack, deg
δ	$P/(10.13\times10^4\ N/m^2)$
θ	T/288.2 K
θ_l	cowl lip position parameter, $\tan^{-1}\left[1/(x/R_c)\right]_{\text{cowl lip}}$
φ	circumferential position, deg

Subscripts:

av	average
bl	bleed
by	overboard bypass
cp	constant pressure
fc	forward cowl
l	local
max	maximum
min	minimum
min s	minimum stable inlet operating point
op	operation
sb	stability bypass
x	value at distance x
0	free stream
5	diffuser-exit station

APPARATUS AND PROCEDURE

Inlet Model

The inlet used in this investigation was a Mach 2.5, axisymmetric, mixed-compression type with 60 percent of the design supersonic area contraction occurring internally. The inlet capture area of 0.1758 square meter sized the inlet to match the airflow requirements of the J85-GE-13 engine at Mach 2.5 and at a free-stream total temperature of 390 K. The inlet was attached to a 0.635-meter-diameter cylindrical nacelle in which either the engine or a coldpipe choked-exit plug assembly could be installed in the test section of the Lewis 10- by 10-Foot Supersonic Wind Tunnel. For this study only the coldpipe was used. Figure 1 shows the test model installed in the wind tunnel test section.

Some of the basic inlet design details are presented in figure 2. Cowl and centerbody static-pressure distributions, inlet contours, and diffuser area variations are shown for the inlet design Mach number and centerbody position. External compression was accomplished with a 12.5° half-angle cone (fig. 3). Translation of this conical centerbody provided a varying contraction ratio to effect inlet restart. At design conditions, the cone tip oblique shock passed just ahead of the cowl lip spilling 0.25 percent of the capture mass flow. Internal compression was accomplished with the oblique shock generated by the 0° cowl lip and the two reflected oblique shocks plus local isentropic compression between the reflected shocks. As was pointed out in reference 8, the actual oblique shock reflection points were forward of the theoretically predicted points. The geometric throat of the inlet was located at $x/R_c = 3.475$ inlet radii (centerbody surface) where the theoretical average supersonic Mach number was 1.239 with a total-pressure recovery of 0.988. Behind the terminal shock the theoretical recovery was 0.975 at a Mach number of 0.8125.

The subsonic diffuser consisted of an initial throat region 4 hydraulic radii long with a 1° equivalent conical expansion followed by the main diffuser having an equivalent conical expansion of 8°. Two remotely controlled bypass systems were installed in the aft portion of the diffuser: (1) a high-response sliding louver overboard system for shock position control and (2) a low-speed ejector bypass for engine and nozzle cooling airflow. For the data reported herein both of these bypass systems were closed. The overboard bypass system leaked about 1 percent of the capture mass flow when nominally closed. The cascades placed at the entrance of the overboard bypass cavity (fig. 3) were found in reference 9 to minimize a resonance condition in the cavity. Vortex generators were installed on the centerbody at inlet station 98.17 (fig. 3). Details of the vortex generator design are shown in figure 4.

The overall diffuser length from cone tip to compressor face was 7.72 cowl lip radii. Internal surface coordinates of the inlet in terms of the cowl lip radius are pre-

sented in table I. A more complete discussion of the inlet design characteristics is presented in reference 8.

Bleed regions were located in the throat region of the inlet on the cowl and centerbody surfaces. As shown in figure 5 the forward cowl bleed airflow was dumped directly overboard. The stability-bypass airflow (used to give the inlet a large stable airflow operating range) was removed through the entrance located in the cowl side of the throat region. Figures 3 and 5 illustrate the ducting of the stability-bypass flow through the cowling to the bypass pipes. The cowl stability-bypass and the centerbody bleed flows each used two coldpipe choked-plug assemblies. The remotely actuated plugs that were used to vary these bleed and bypass flows as well as the main duct flow are shown in figure 1(b).

The photographs and sketches of the test model show a bulky external profile. The bulky cowl was necessary to facilitate the major changes made to the stability bypass and associated ducting to vary the entrance configurations, hence, it is not representative of flight type hardware.

Stability-Bypass Entrance and Bleed Region

The centerbody bleed region was composed of rows of normal holes (fig. 6). There were five rows of holes aft of the inlet throat and eight rows forward of the throat. The holes in the forward rows were arranged in a concentrated, staggered pattern. The intent of staggering was to prevent axial strips of unbled surface that might induce circumferential variations in the boundary layer.

The bleed characteristics contained in references 10 to 12 were used to design the distributed educated stability-bypass entrance (fig. 7). The educating technique used was an approximation of the ideal rearward slanted hole concept explained in the appendix. The rearward slant or education theoretically limits the amount of airflow through the slanted holes when the flow over a perforated area is supersonic. With subsonic flow over a perforated area the airflow through the holes is relatively unaffected by the slant, and a flow coefficient nearly equal to a normal hole value is achieved. Because of the difficulty of drilling slanted holes in the cowl surface, a number of circumferential slots were used rather than many holes (fig. 7). To educate these slots, the downstream edge was relieved to obtain a 10° angle with the local surface. The slot width was 0.318 centimeter with 1.27 centimeters between adjacent slots. Local porosity resulting from this arrangement was 25 percent and resulted in an estimated maximum stability-bypass mass-flow ratio capability of 17 percent.

The forward cowl bleed region was also composed of educated slots (see fig. 7). The forward cowl bleed region was included for cowl side boundary-layer control purposes.

The complete distributed educated stability bypass configuration tested is shown in figure 8. The selected bleed and stability-bypass entrance patterns were constructed by filling in the appropriate normal holes and slots. The centerbody bleed pattern used was identical to the final pattern presented in reference 5. This particular bleed pattern provided the best stability performance of those tested and reported in that reference.

Instrumentation

Static-pressure distributions along the top centerline of the inlet cowl and centerbody were measured by the axially located static-pressure instrumentation presented in tables II and III. The main-duct total-pressure instrumentation (fig. 9) was used to determine the local flow profiles through the inlet and subsonic diffuser. The axial locations of these total-pressure rakes are shown in figure 3. Overall inlet total-pressure recovery and distortion were determined from the six 10-tube total-pressure rakes that were located at the diffuser exit (fig. 9(b)). Each rake consisted of six equal-area-weighted tubes with additional tubes added at each side of the extreme tubes. These additional tubes were in radial positions corresponding to an 18-tube area-weighted rake.

The main duct airflow, the stability-bypass airflow, and the centerbody bleed airflow were determined from static-pressure measurements and the appropriate coldpipe choked-plug areas. Bleed flow through the forward cowl bleed region was determined from the measured total and static pressures (fig. 9(c)) and the bleed exit area.

Stability-bypass total pressure was obtained from two total-pressure rakes that were located in the bypass plenum at an x/R_c of 4.086 inlet radii. Pressures from these rakes were averaged to obtain the stability-bypass recovery. Centerbody bleed and overboard-bypass total pressures were each measured by a single probe as indicated in figure 9(c).

PERFORMANCE ANALYSIS TECHNIQUE

This section of the report introduces stylized plots (fig. 10) that are typical of actual inlet stability data presented later. These plots are used to explain the data presentation and to show the method used to construct a final performance plot. Various performance conditions have been labelled in figure 10 to aid in the discussion.

The stability-bypass performance is shown in figure 10(a) where the total-pressure recovery is presented as a function of the mass-flow ratio of the stability bypass. The series of straight solid lines (A'AB, C'CD etc.) represent the bypass performance obtainable with several different fixed bypass exit areas. Corresponding inlet performance is presented in figure 10(b) by a series of standard diffuser-exit total-pressure recovery

against mass-flow ratio curves. The diffuser-exit mass-flow ratio, of course, reflects the changes in bypass mass-flow ratio and also changes in forward cowl and centerbody bleed mass-flow ratios. Each solid-line curve represents the performance obtainable with a fixed bypass exit area and corresponds to the solid straight line of identical labelling in figure 10(a). Each of these curves is generated by reducing the inlet diffuser-exit corrected airflow from a supercritical value and thus causing the inlet terminal shock to move upstream until unstart occurs. By this mode of operation, loci of supercritical stability-bypass airflow (A'A C'C E'E G'G) and minimum stable bypass airflow (BDFH) are obtainable. For a given bypass exit area all the supercritical inlet operating points have approximately the same bypass mass-flow and pressure-recovery values. Only when the terminal shock is in the vicinity of the stability-bypass entrance region will shock pressurization occur, causing increases in the bypass mass flow and pressure recovery toward their respective minimum stable limit values. Thus for example all the inlet operating points between A' and A of figure 10(b) will have the same stability-bypass performance point, which is labelled as A'A in figure 10(a).

To assess inlet stability, it is necessary to look at the change in the diffuser-exit corrected airflow, which is a function of both diffuser-exit mass-flow ratio and total-pressure recovery. Figure 10(c) presents inlet stability, expressed as an airflow index, for the same conditions of figures 10(a) and (b). Values of airflow index (AI) represent the percentage change in corrected airflow between any inlet operating condition and the minimum recorded corrected airflow at point H. Figure 10(c) thus illustrates the amount of stable margin available if the stability-bypass exit area can be varied to guide the inlet operation from any operating condition to an unstart at point H. If a fixed exit area were used to obtain the large stability-bypass airflow available at point H (fig. 10(a)), a prohibitively large amount of bypass airflow would be removed from the diffuser flow at supercritical conditions (point G). If the fixed exit area were reduced to obtain an acceptably low level of supercritical bypass airflow (point C), the amount of bypass airflow and consequently the stable margin at the minimum stable condition (point D) would also be reduced. Similar bypass characteristics are reported in references 1 to 4.

Data such as that presented in figures 10(a) to (c) show the characteristic performance of an inlet with a stability-bypass entrance. Since a performance assessment from these plots is difficult, a single operating line was chosen to represent the configuration performance. One end of the line represents a high-performance operating point that matches the inlet and an assumed engine and will be called the match point (point A, for example). The match point was chosen to have a high inlet recovery and a small amount of cowl side airflow removal for boundary-layer control. The other end of the operating line (the minimum stable point) was chosen by the selection of an ideal variable exit area, one that would provide a constant pressure in the bypass plenum as the inlet operated from the match point to the minimum stable point. This variable exit area

provides the maximum attainable stability (points A to M in fig. 10(a)). Reference 4 reports a pressure-activated valve that varied the stability-bypass exit area to maintain an almost constant bypass plenum pressure. Thus the selection of a constant pressure characteristic for a stability-bypass exit control is a valid technique for assessing inlet stability performance.

The inlet stability margin that is produced by a constant-pressure bypass-exit-area control is expressed as a stability index SI_{cp}. Figure 10(d) presents the constant-pressure stability index for all of the operating points of figures 10(a) to (c). Note that the selected match point stability (A to M on figs. 10(a) to (c)) is now represented by a single point A. The values of stability index at any operating point represent the percentage change in corrected airflow between that point and a minimum stable point that is reached only along a line of constant stability-bypass pressure recovery (A to M in fig. 10(a)). When the inlet operating point has a stability-bypass recovery lower than that of the absolute minimum stable point (H in fig. 10(a)), the absolute minimum stable point is used to compute the stability index. Therefore, the stability index for the lower bypass recovery conditions in figure 10(d) becomes identical to the airflow index in figure 10(c). Although the stability index is defined in terms of corrected airflow, that is,

$$SI_{cp} = 100\left[1 - \frac{(W\sqrt{\theta}/\delta)_{\text{min s, cp}}}{(W\sqrt{\theta}/\delta)_{op}}\right] \tag{1}$$

it was easier in practice to determine values of stability index directly from curves of airflow index by means of the following equation:

$$SI_{cp} = 100\left(\frac{AI_{op} - AI_{\text{min s, cp}}}{100 - AI_{\text{min s, cp}}}\right) \tag{2}$$

where AI_{op} is the airflow index at any inlet operating condition and $AI_{\text{min s, cp}}$ is the airflow index at the corresponding minimum stable point assuming a constant bypass recovery is maintained.

Constant-pressure stability index levels may be converted into typical inlet performance plots like that of figure 10(g) by means of figures 10(e) and (f). Figure 10(e) presents the constant pressure stability index that was computed for each inlet operating condition as a function of inlet total-pressure recovery. A selected inlet total-pressure recovery may be represented on figure 10(e) as a vertical line (LJKL). (Note that point A is no longer necessarily the selected match point. The choice of inlet recovery and the amount of performance bleed will dictate the match point.) The intersection of this line with the lines of constant bypass exit area indicate the constant-pressure stability indices

available at the selected inlet recovery for the various bypass exit areas. A replot of these data in figure 10(f) shows the amount of stability margin that is available when operating the inlet at the selected match recovery as a function of the various amounts of initial total forward cowl bleed and stability-bypass mass flow. Any of the data points in figure 10(f) may be converted into a typical inlet performance plot. Point J, for example, is shown in figure 10(g) and is determined by the previously selected inlet recovery and the initial amount of total mass flow removed through the cowl surface. If point J represents critical inlet performance, then supercritical performance is represented by a vertical line extended below point J. The constant-pressure stability index for point J as determined by equation (1) is represented by the airflow difference between two corrected airflow lines: one through the selected match point $(W\sqrt{\theta}/\delta)_{op}$ and the other $(W\sqrt{\theta}/\delta)_{min\ s,\ cp}$ intersecting the locus of minimum stable conditions in the inlet performance map (fig. 10(b)). For convenience, inlet performance between the match point and the minimum stable point is represented by a straight line. Intermediate points could be determined by using figures 10(a) through (d).

RESULTS AND DISCUSSION

The results of this investigation are presented in two parts: the stability performance of the configuration and the unstart angle-of-attack tolerance of the configuration.

Stability Performance

The overall performance curves for the distributed educated configuration tested are presented in figure 11. Cowl and centerbody static-pressure distributions and total-pressure profiles at the various survey stations are presented in figure 12 for the minimum stable inlet operating conditions and in figure 13 for representative inlet supercritical operating conditions. Only profiles for rake 5 of the six diffuser-exit rakes will be presented herein as this profile was found to be representative of all rakes. Note that throughout this report an attempt has been made to maintain consistency in the figure symbols; that is, the same symbol used to represent a particular fixed bypass exit area in the stability-bypass performance curves (i. e., fig. 11(a)) is also used in the inlet performance curves (i. e., figs. 11(b) to (j)) and in the pressure distribution and profile figures (i. e., figs. 12 and 13).

The performance of the distributed educated entrance configuration is presented in figure 11(a). The curves indicate that the maximum stability bypass total-pressure recovery recorded was about 0. 62 and that the maximum bypass mass-flow ratio attained was about 0. 12. The bypass recovery at the maximum bypass mass flow was quite low,

being only 0. 19. The trend of the curves of figure 11(a) for supercritical inlet operation reveals that educating the entrance region did result in small amounts of bypass mass flow when the local diffuser flow was supersonic. The maximum supercritical bypass mass-flow ratio recorded was only 0. 065. Also the bypass recovery dropped rapidly with an increase in supercritical bypass mass flow. As discussed previously, a reason for educating a bleed region is to reduce the amount of bleed flow when the external flow is supersonic. Certainly, the distributed educated entrance configuration exhibited such a desirable characteristic. However, the curves of figure 11(a) also reveal that the bypass recovery dropped rapidly with increased bypass mass flow at the minimum stable conditions. Such a loss in bypass recovery deviated from the expected result of educating the entrance region, that being high recovery levels and large mass flows when the external flow is subsonic.

The less than desirable performance of the educated configuration at the minimum stable conditions indicates the allowable increase in stability-bypass mass flow at a given bypass pressure recovery before an inlet unstart occurring would be restricted. This limitation on the maximum allowable bypass flow is evident in the levels of constant-pressure stability index achieved by the educated configuration as shown in figure 11(f). The maximum stability index achieved was approximately 16. 1 percent and corresponded to an initial total mass-flow ratio removed through the cowl of about 0. 023. For larger amounts of flow removal, the stability index continually decreased, reaching a value of 12 percent when 0. 114 mass-flow ratio was removed through the cowl surface. The levels achieved do represent a sizeable increase in stability performance over the 6 to 9 percent levels quoted in reference 8 for a fixed exit performance bleed system in the same inlet. It must be pointed out that the diffuser-exit pressure recovery chosen to construct figure 11(f) was 0. 89. This level of performance was indicative of the achievable pressure recovery exhibited by the inlet regardless of the particular bypass entrance used.

The choice of the 0. 023 total forward cowl bleed and stability-bypass mass-flow ratio and resulting stability index of 16. 1 percent allows the performance curve of figure 11(g) to be constructed. The curve indicates that, if a constant pressure level is maintained by the bypass plenum, a minimum stable point of 0. 94 inlet pressure recovery and 0. 85 diffuser-exit mass-flow ratio would be reached. From figure 11(a) the corresponding constant pressure level maintained in the bypass plenum would be about 0. 32, and the increase in stability-bypass mass-flow ratio before unstart would be about 0. 08.

To achieve the maximum stability index, figure 11(f) indicates that it was necessary to remove about 0. 023 mass-flow ratio through the forward cowl and stability-bypass regions of which about 0. 015 mass-flow ratio must be removed through the stability-bypass system (see figs. 11(a) and (b)). The necessity of removing additional flow through the stability-bypass system beyond the small amount of performance bleed re-

moved through the forward cowl in order to achieve maximum stability performance will result in an increased bleed drag penalty to be paid at the initial inlet operating condition.

The cowl and centerbody surface static-pressure distributions for the minimum stable operating points are shown in figures 12(a) and (b). These distributions indicate that the terminal shock could be positioned well forward of the geometric throat before unstart. The centerbody distributions of figure 12(b) indicate that at the higher minimum stable stability-bypass flows, a distinct change in pressure trend (indicative of flow separation) occurred. The corresponding centerbody boundary-layer rake profiles of figure 12(c) also indicate that a definite flow reversal did occur ahead of the centerbody bleed region. The throat-exit rake profiles of figure 12(d) indicate the flow had reattached before reaching that station; however, low-energy flow near the centerbody surface still existed. The corresponding diffuser-exit rake profiles of figure 12(f) reveal that the flow had fully recovered before reaching the engine face. It might be noted that the characteristics of the mid-diffuser rake profiles (fig. 12(e)) are due to placing the rake close to the vortex generators.

A similar centerbody flow separation phenomenon was reported in references 5 and 6 for the same general inlet but with different stability-bypass entrance configurations. Also, reference 8, which reported on a study of the same inlet with only performance bleed, showed that a similar separation was caused by the terminal shock being positioned forward of the geometric throat. This separation in contrast to what one might expect was of a small-scale nature and did not affect overall inlet performance. Further tailoring of the centerbody bleed pattern could possibly have prohibited the separation from occurring at the higher stability-bypass flows. However, as noted previously, the bleed pattern used for the test reported herein was identical to the final pattern reported in reference 5.

Unstart Angle-of-Attack Tolerance

The unstart angles of attack for critical and supercritical initial operating conditions are shown on the inlet performance curves of figure 11(b). The angles listed (3.7° and 3.8°) represent the maximum steady-state angle of attack the configuration could tolerate before unstart. Both angles of attack given herein correspond to conditions of no flow through the stability-bypass entrance. The only cowl side flow removal was through the forward cowl bleed region; thus, all bleed flows were for performance purposes.

In a separate study of the same inlet, but with performance bleed only (ref. 13), it was determined that unstarts at angle of attack were caused by an overcompression of the flow field on the leeward side of the inlet. This overcompression resulted in a local choking of the flow forward of the geometric throat. Figure 14 presents the static-

pressure distributions for both the cowl and centerbody surfaces at 3.8° operation. For reference, the initial 0° angle-of-attack operating-point pressure distributions are also shown. The cowl surface distribution of figure 14(a) reveals a region forward of the geometric throat where the pressure ratio rose well above the sonic value of 0.5283 (assuming isentropic conditions). In addition the profiles indicate that the terminal shock was located well downstream of the geometric throat. The static-pressure distributions for the other unstart angle-of-attack operating point show the same trends. Thus it appears that a leeward side overcompression and resulting flow choking caused the angle-of-attack unstarts recorded.

The unstart angles of attack that were achieved by this configuration are about the same as the levels that were reported in references 8 and 13, which, as noted previously, used the same inlet but different performance bleed configurations. Thus it appears that the inclusion of a stability-bypass system with the required entrance configuration did not affect the inlet's basic angle-of-attack tolerance. This was the expected result because the overcompression and local choking occurred upstream of the stability-bypass entrance.

SUMMARY OF RESULTS

An experimental program was conducted in the Lewis 10- by 10-Foot Supersonic Wind Tunnel to evaluate the effectiveness of a distributed educated stability-bypass entrance configuration in providing an increased inlet stable corrected airflow operating range. The inlet used in the investigation was an axisymmetric, mixed-compression type with 60 percent of the supersonic area contraction occurring internally at the design Mach number of 2.50.

The following results were obtained:

1. A large stable airflow operating range could be provided for the inlet operating at high-performance conditions by maintaining a nearly constant plenum pressure in an inlet stability-bypass system. From initial inlet operating conditions of 89-percent diffuser-exit pressure recovery and a total forward cowl bleed and stability-bypass mass-flow ratio of 0.023, the diffuser-exit corrected airflow could be reduced 16.1 percent before unstart.

2. Educating the stability-bypass entrance region achieved the desired result of maintaining low bypass mass flows for supercritical inlet operating conditions. However, the bypass recovery also dropped rapidly for minimum stable conditions as the bypass mass flow increased, limiting the effectiveness of the configuration in providing inlet stability.

3. Inlet unstart angle-of-attack tolerance varied from 3.7° to 3.8°, depending on the initial operating conditions. These levels were commensurate with the results de-

termined for the same inlet without the inclussion of any throat stability-bypass system. In all cases the unstarts incurred from angle-of-attack operation resulted from local flow choking forward of the geometric throat on the leeward side of the inlet.

Lewis Research Center,
National Aeronautics and Space Administration,
Cleveland, Ohio, December 12, 1973,
501-24.

APPENDIX - "EDUCATED" HOLE DESIGN

The so-called "educated" hole was developed by past experimenters (e.g., ref. 14) with the idea of limiting the flow through a perforated wall when the flow past the wall was at supersonic speeds. No restriction on the flow was desired at subsonic speeds. The theoretical aspects of such a hole design begin with a consideration of the flow patterns generated when supersonic flow approaches a sharp edged hole (see sketch (a)). This flow was analyzed first in reference 15.

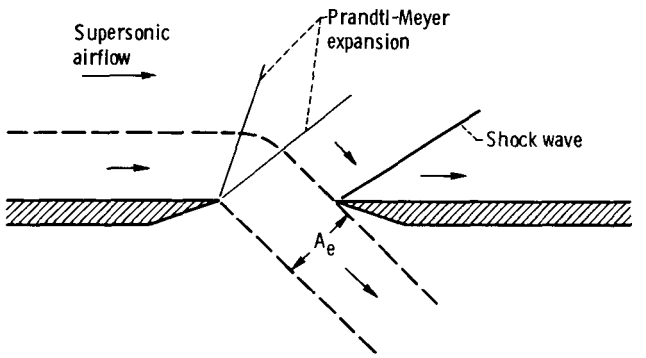

(a) Conventional hole

Flow through the hole occurs at an angle that is the difference between the Prandtl-Meyer expansion angles of the exiting flow and the approaching supersonic flow.

A rearward slant of the downstream hole edge (i.e., "education") can limit hole outflow as shown in sketch (b).

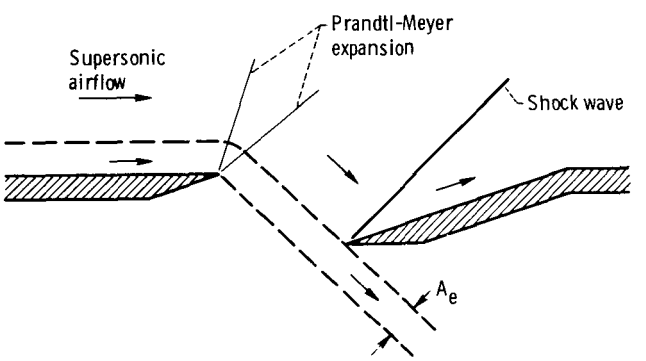

(b) "Educated" hole

The supersonic expansion waves again control the turn of the flow into the hole. But with the drooped or relieved downstream hole edge, the turn is not sufficient to pass all the flow within the original exiting streamline ahead of the downstream edge. The effective exit area A_e is reduced, and the outflow is restricted. With subsonic flow approaching the hole, flow turning is not limited as with supersonic flow, and the "educated" hole should act like a conventional hole.

These theoretical flow patterns are, of course, modified by practical realities such as the wall boundary layer and the structural necessity of thicker walls and blunter hole edges. The basic effects of "education" can still be realized, however. Reference 14 reports the experimental performance of three "educated" hole configurations at a Mach number of 1.45. Flow through the "educated" holes was approximately one-half of that allowed by normal holes.

A generalized sketch of the "educated" slot configuration discussed in the main text of this report is shown in sketch (c).

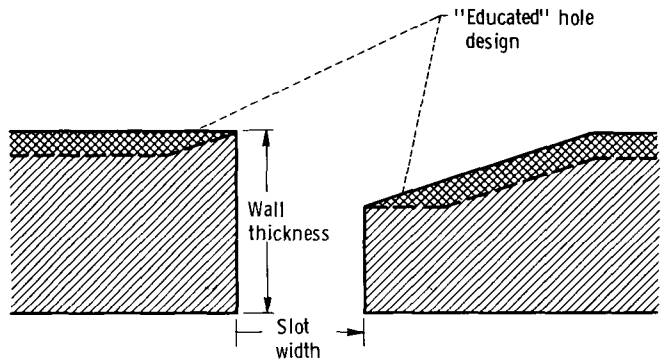

(c) "Educated" slot

As is evident from sketch (c), in this slot configuration the basic "educated" hole geometry was used but the design was modified by adding thickness to the wall for structural and fabrication purposes.

REFERENCES

1. Sanders, Bobby W.; and Cubbison, Robert W.: Effect of Bleed-System Back Pressure and Porous Area on the Performance of an Axisymmetric Mixed-Compression Inlet at Mach 2.50. NASA TM X-1710, 1968.

2. Sanders, Bobby W.; and Mitchell, Glenn A.: Throat-Bypass Bleed Systems for Increasing the Stable Airflow Range of a Mach 2.50 Axisymmetric Inlet with 40-Percent Internal Contraction. NASA TM X-2779, 1973.

3. Sanders, Bobby W.; and Mitchell, Glenn A.: Increasing the Stable Operating Range of a Mach 2.5 Inlet. Paper 70-686, AIAA, June 1970.

4. Mitchell, Glenn A.; and Sanders, Bobby W.: Pressure-Activated Stability-Bypass-Control Valves to Increase the Stable Airflow Range of a Mach 2.5 Inlet with 40-Percent Internal Contraction. NASA TM X-2972, 1974.

5. Shaw, Robert J.; Mitchell, Glenn A.; and Sanders, Bobby W.: Distributed Porous Throat Stability Bypass to Increase the Stable Airflow Range of a Mach 2.5 Inlet with 60-Percent Internal Contraction. NASA TM X-2974, 1974.

6. Shaw, Robert J.; Mitchell, Glenn A.; and Sanders, Bobby W.: Forward-Slanted Slot Throat Stability Bypass to Increase the Stable Airflow Range of a Mach 2.5 Inlet with 60-Percent Internal Contraction. NASA TM X-2973, 1974.

7. Mitchell, Glenn A.; Sanders, Bobby W.; and Shaw, Robert J.: Throat Stability-Bypass Systems to Increase the Stable Airflow Range of a Mach 2.5 Inlet with 60-Percent Internal Contraction. NASA TM X-2976, 1974.

8. Cubbison, Robert W.; Meleason, Edward T.; and Johnson, David F.: Effect of Porous Bleed in a High-Performance Axisymmetric, Mixed-Compression Inlet at Mach 2.50. NASA TM X-1692, 1968.

9. Coltrin, Robert E.; and Calogeras, James E.: Supersonic Wind Tunnel Investigation of Inlet-Engine Compatibility. Paper 69-487, AIAA, June 1969.

10. McLafferty, George: A Stepwise Method for Designing Perforated Supersonic Diffusers. Rep. R-12133-5, United Aircraft Corp., Nov. 17, 1949.

11. McLafferty, George: Study of Perforation Configurations for Supersonic Diffusers. Rep. R-53372-7, United Aircraft Corp., Dec. 1950.

12. McLafferty, George; and Ranard, E.: Pressure Losses and Flow Coefficients of Slanted Perforations Discharging From Within a Simulated Supersonic Inlet. Rep. R-0920-1, United Aircraft Corp., 1958.

13. Choby, David A.: Tolerance of Mach 2.50 Axisymmetric Mixed-Compression Inlets to Upstream Flow Variations. NASA TM X-2433, 1972.

14. Goethert, Bernhard H.: Transonic Wind Tunnel Testing. Pergamon Press, 1961.

15. Evvard, John C.; and Blakey, John W.: The Use of Perforated Inlets for Efficient Supersonic Diffusion. NACA TN-3767, 1956.

TABLE I. - INLET INTERNAL SURFACE COORDINATES

(a) Centerbody

Axial distance from cone tip, x/R_c, inlet radii	Radial distance, r/R_c, inlet radii	Axial distance from cone tip, x/R_c, inlet radii	Radial distance, r/R_c, inlet radii
0	0	4.563	0.588
(a)	(a)	4.724	.566
2.885	.640	5.161	.498
2.924	.649	5.261	.481
2.952	.655	5.361	.462
3.017	.667	5.461	.444
3.081	.678	5.561	.418
3.124	.684	5.661	.409
3.178	.691	5.761	.396
3.221	.696	5.861	.373
3.237	.700	5.961	.357
3.306	.703	6.061	.341
3.349	.705	6.161	.327
3.403	.707	6.261	.313
3.435	.708	6.361	.299
3.446	↓	6.461	.285
3.457	↓	6.561	.272
3.468	↓	6.661	.260
3.478	.707	6.761	.250
3.489	.706	6.861	.243
3.543	.702	8.961	.240
3.596	.697	7.061	.239
3.650	.691	Cylinder	
3.865	.670	7.946	0.239
3.972	.660		
4.079	.649		
4.120	.644		
4.187	.636		
4.240	.635		
4.294	.623		
4.402	.609		

[a] 12.5^{o} Half angle conical section.

TABLE I. - Concluded. INLET INTERNAL SURFACE COORDINATES

(b) Cowl

Axial distance from cone tip, x/R_c, inlet radii	Radial distance, r/R_c, inlet radii	Axial distance from cone tip, x/R_c, inlet radii	Radial distance, r/R_c, inlet radii
2.009	1.000	4.267	0.906
2.156	↓	4.277	.905
2.297		4.384	.903
2.383		4.545	.902
2.469		4.706	.902
2.491		4.868	.903
2.512		5.029	.904
2.566	.999	5.093	.904
2.630	.997	5.161	.905
2.695	.995	5.261	.907
2.738	.994	5.361	.910
2.811	.992	5.461	.913
2.860	.989	5.561	.916
2.885	.988	5.661	.917
2.924	.986	5.761	.918
2.952	.985	Cylinder	
3.017	.981		
3.081	.979	6.235	0.918
3.124	.976		
3.178	.972	Bypass gap	
3.221	.971		
3.237	.966	6.845	0.887
3.306	.963	6.861	.887
3.350	.960	6.961	.885
3.403	.955	7.061	.882
3.435	.953	7.161	.879
3.446	.952	7.261	.873
3.457	.951	7.361	.868
3.468	.951	7.461	.864
3.478	.950	7.561	.863
3.489	.949	7.661	.862
3.543	.945	Cylinder	
3.596	.942		
3.650	.939	7.946	0.862
3.756	.932		
3.863	.925		
3.970	.919		
4.088	.913		
4.093	.913		
4.189	.909		

TABLE II. - COWL STATIC PRESSURE TAP LOCATIONS ALONG TOP CENTERLINE

Axial distance from cone tip, x/R_c, inlet radii	
2.983	3.662
3.090	3.739
3.194	3.818
3.203	3.961
3.257	4.254
3.310	-----
3.364	-----
3.418	-----
3.471	-----
3.525	-----
3.579	-----
3.620	-----

TABLE III. - CENTERBODY STATIC PRESSURE TAP LOCATIONS ALONG TOP CENTERLINE

Axial distance from cone tip, x/R_c, inlet radii		
2.806	3.367	3.854
2.920	3.402	3.906
3.022	3.440	3.961
3.136	3.470	4.067
3.173	3.510	4.174
3.206	3.573	4.331
3.242	3.635	-----
3.272	3.691	-----
3.315	3.741	-----
3.332	3.798	-----

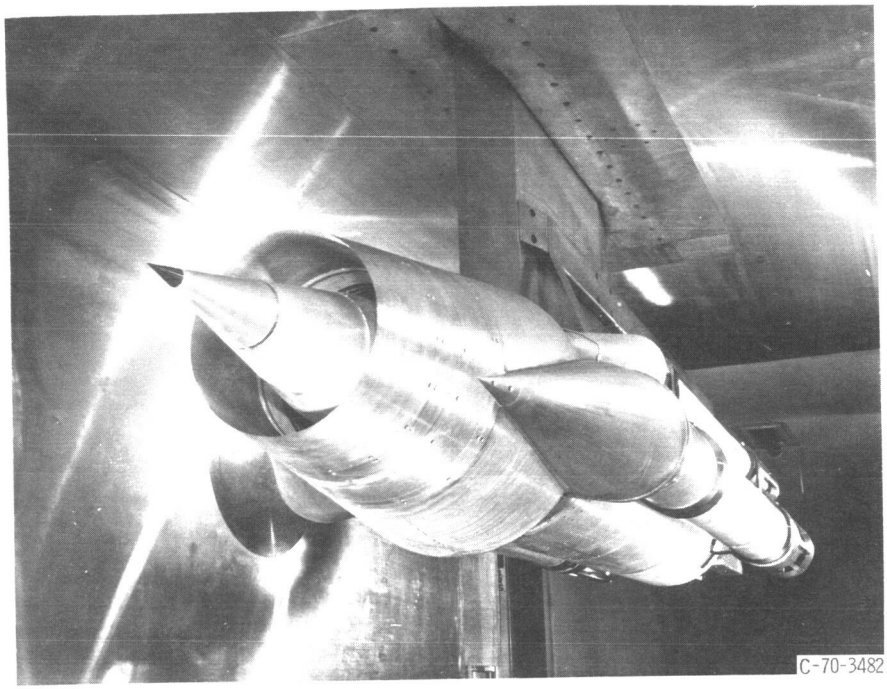

(a) Front view.

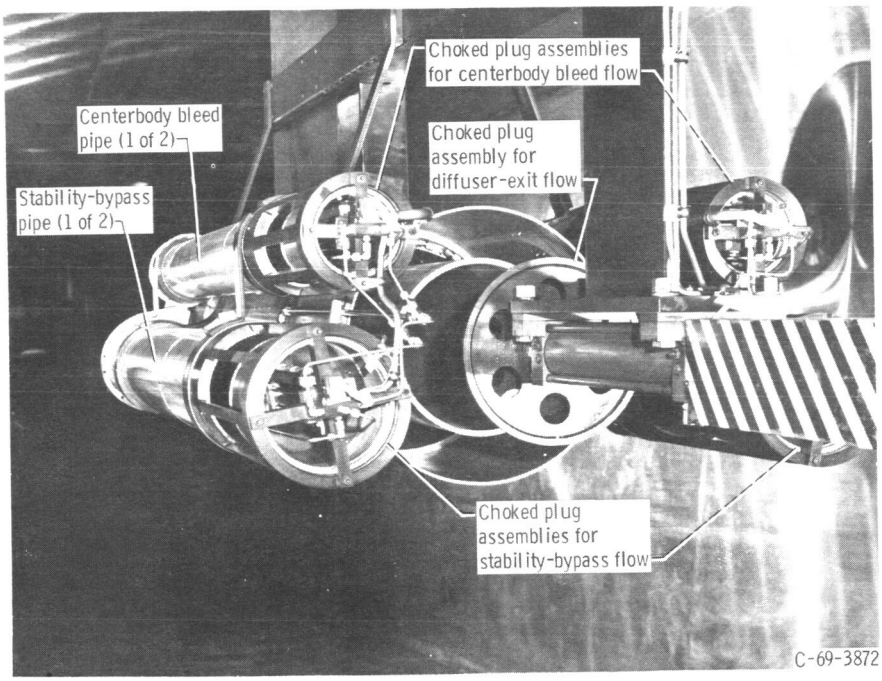

(b) Rear view.

Figure 1. - Model installed in wind tunnel.

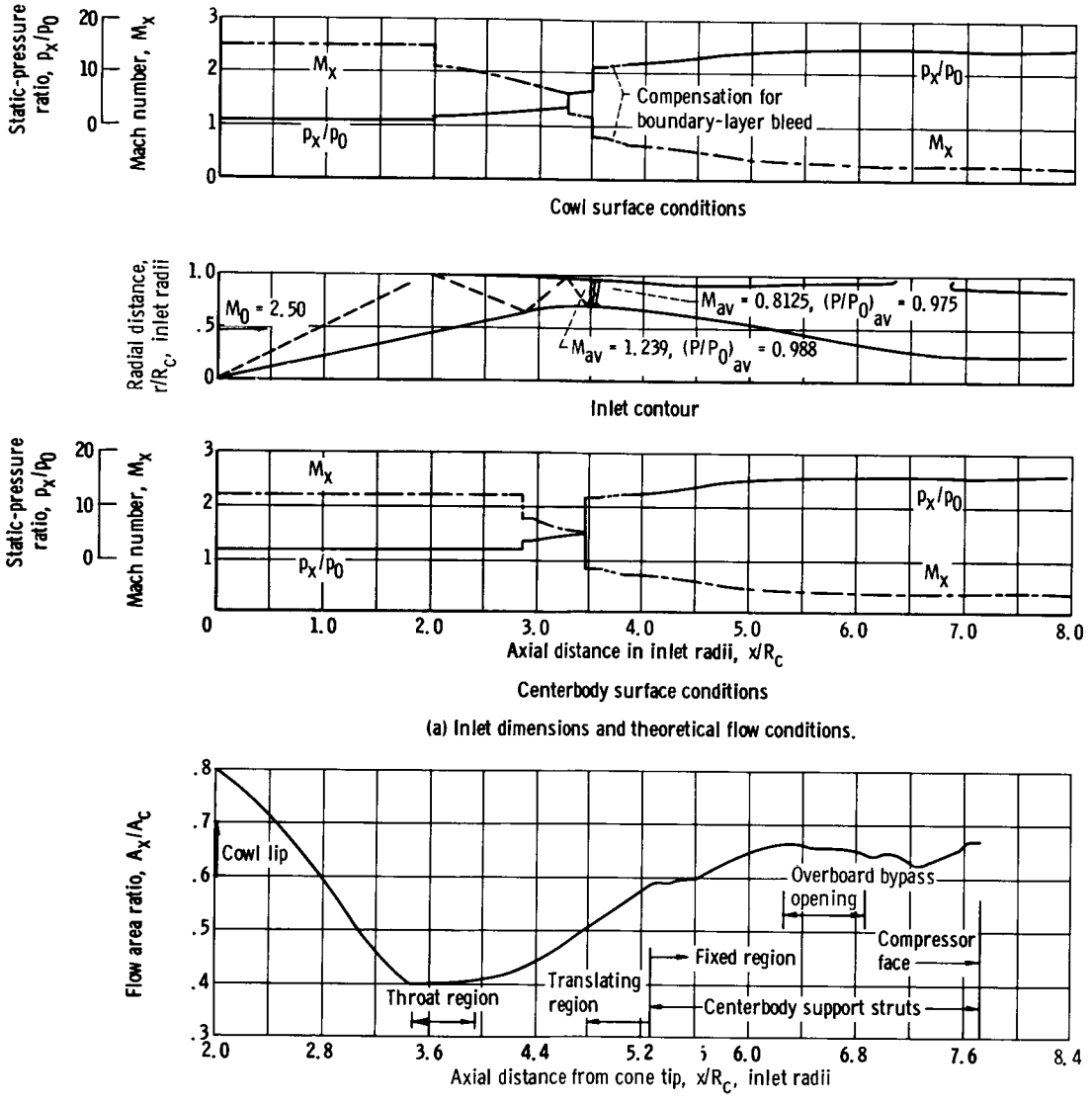

(a) Inlet dimensions and theoretical flow conditions.

(b) Diffuser area variation for θ_l, 26.72°.

Figure 2. - Aerodynamic details.

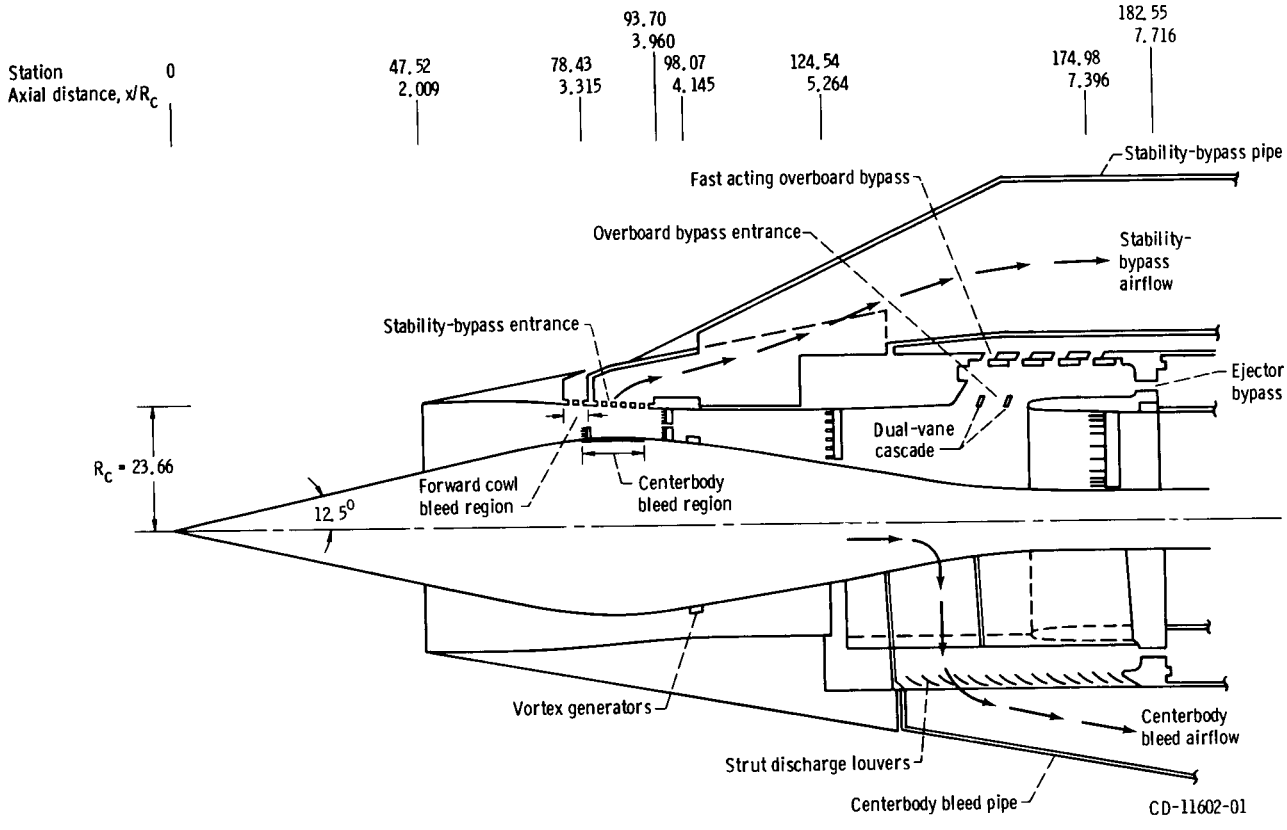

Figure 3. - Inlet details. (All linear dimensions are in cm.)

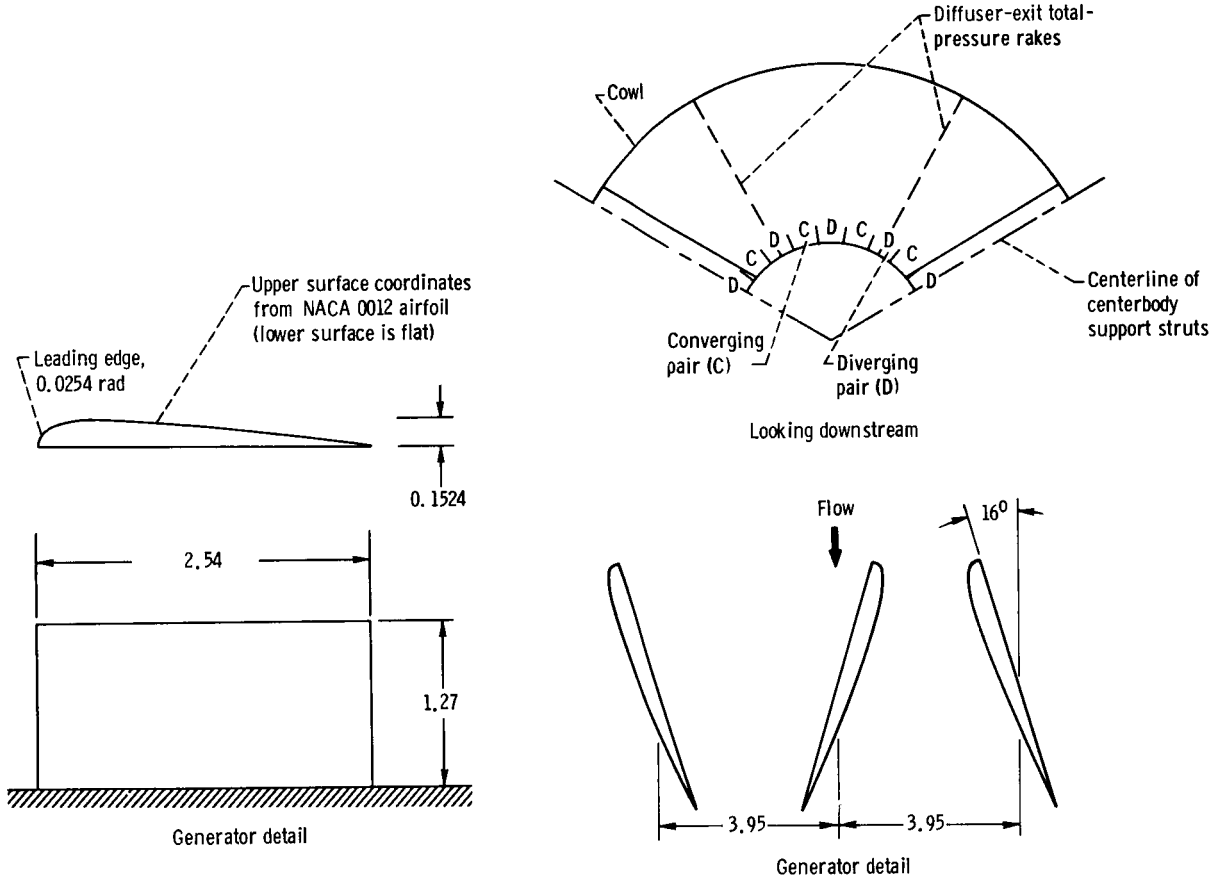

Figure 4. - Vortex generator design. (All linear dimensions are in cm.)

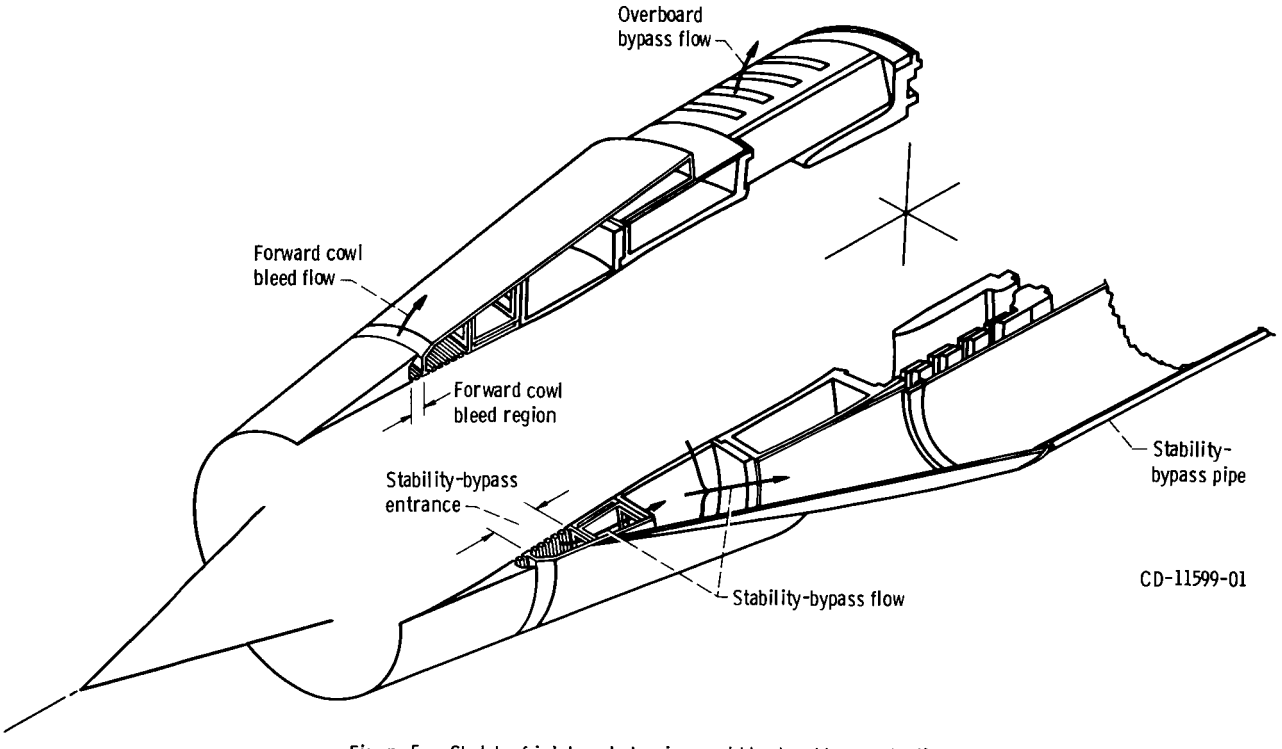

Figure 5. - Sketch of inlet cowl showing cowl bleed and bypass ducting.

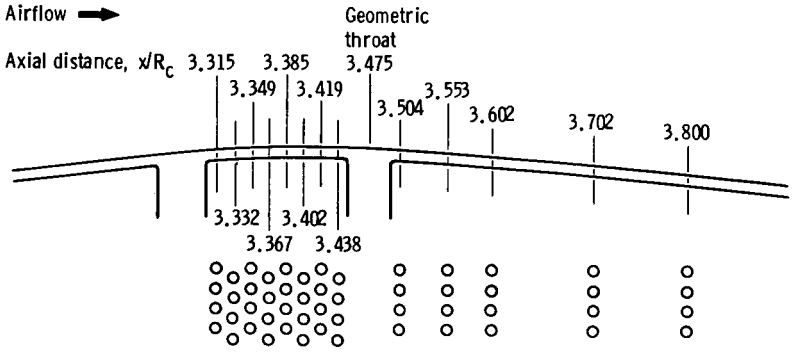

Figure 6. - Centerbody bleed arrangement. Hole diameter, 0.3175 centimeter.

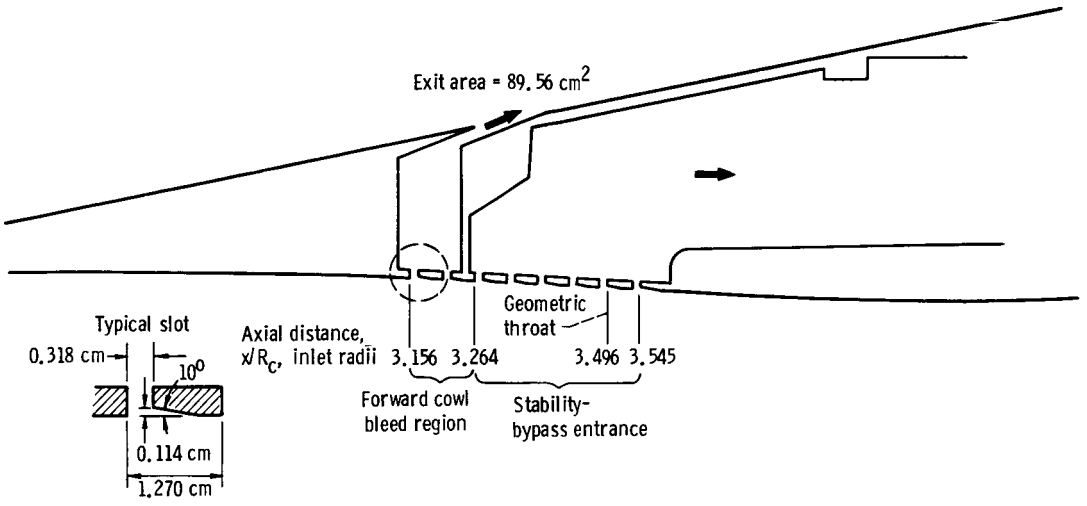

Figure 7. - Distributed educated stability-bypass entrance.

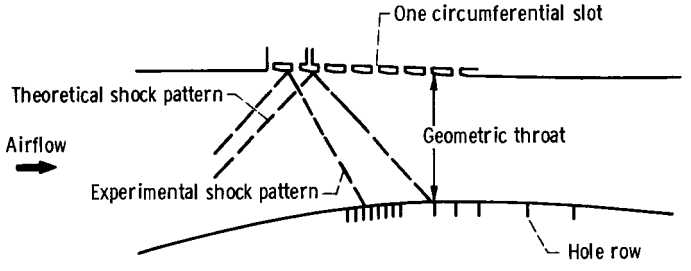

Configuration	Forward cowl bleed region	Distributed educated stability-bypass entrance	Centerbody bleed region
ED	■□	■□□□□□	○○○○○○●● ●●● ●●

□ Slot open
■ Slot closed
○ Hole row open
● Hole row closed

Figure 8. - Inlet stability-bypass entrance and bleed region configuration.

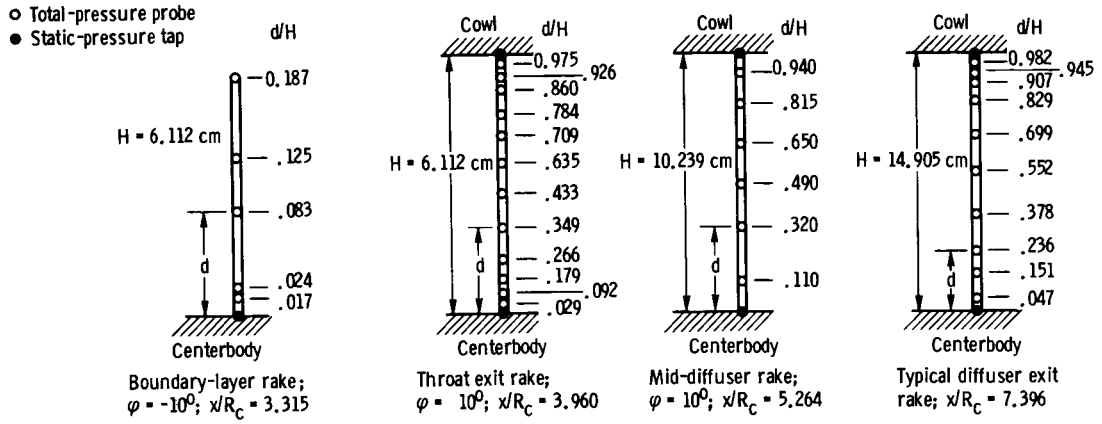

(a) Inlet-total-pressure rake dimensions.

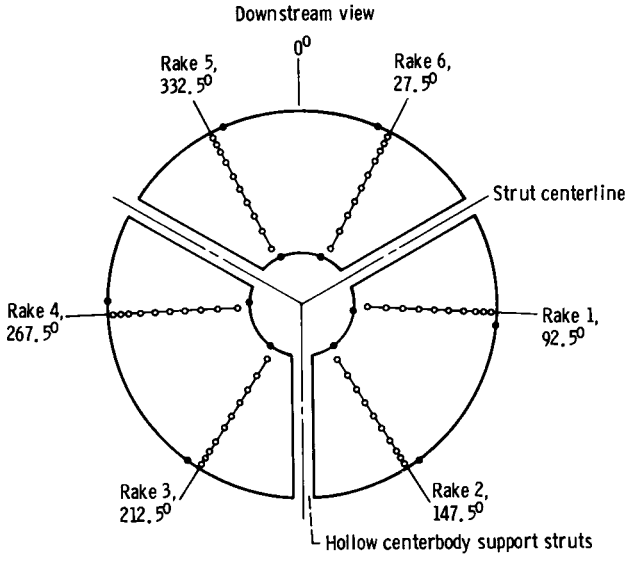

(b) Total- and static-pressure instrumentation at diffuser-exit station, $x/R_c = 7.396$.

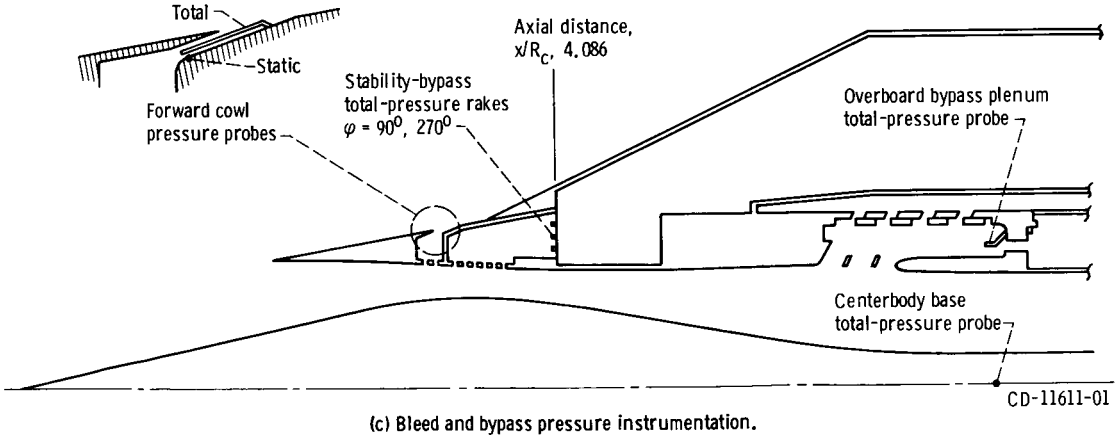

(c) Bleed and bypass pressure instrumentation.

Figure 9. - Inlet-pressure instrumentation (x/R_c is the axial distance from cone tip, φ is the circumferential position, and d/H is the ratio of distance from surface to annulus height).

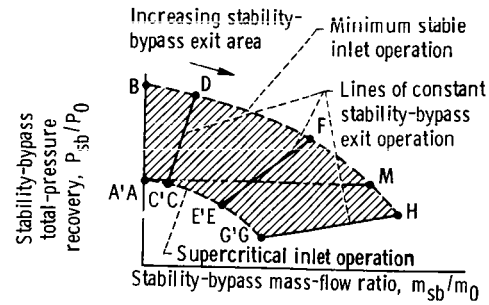

(a) Stability-bypass performance.

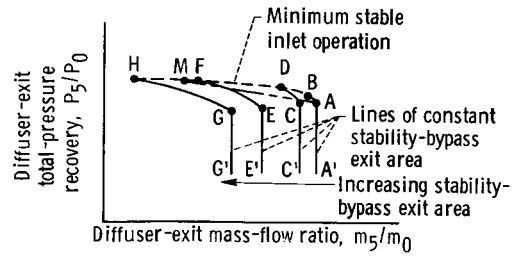

(b) Inlet performance.

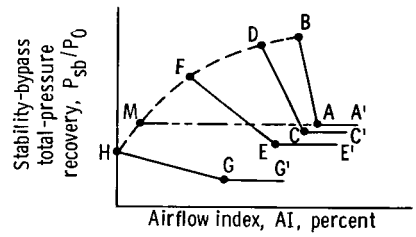

(c) Airflow index.

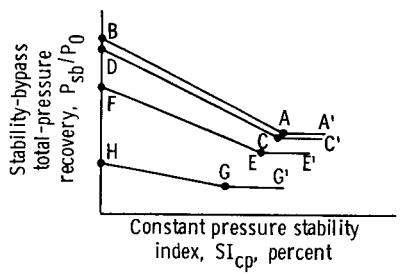

(d) Stability index for constant stability-bypass recovery.

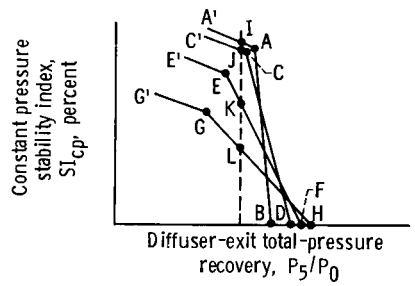

(e) Variation of constant pressure stability index with diffuser-exit total-pressure recovery.

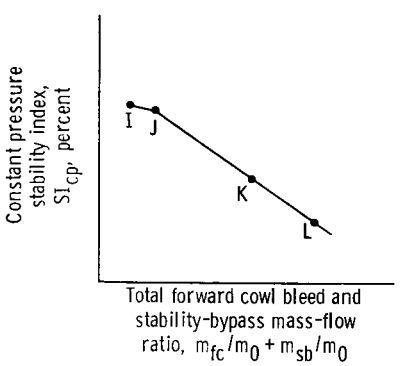

(f) Constant pressure stability index for chosen inlet total-pressure recovery.

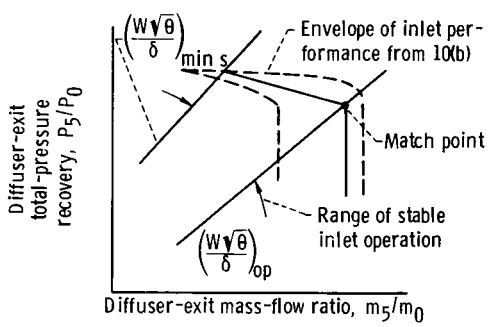

(g) Inlet performance for point J as match condition and with constant pressure bypass-exit control on stability bypass airflow.

Figure 10. - Inlet stability data.

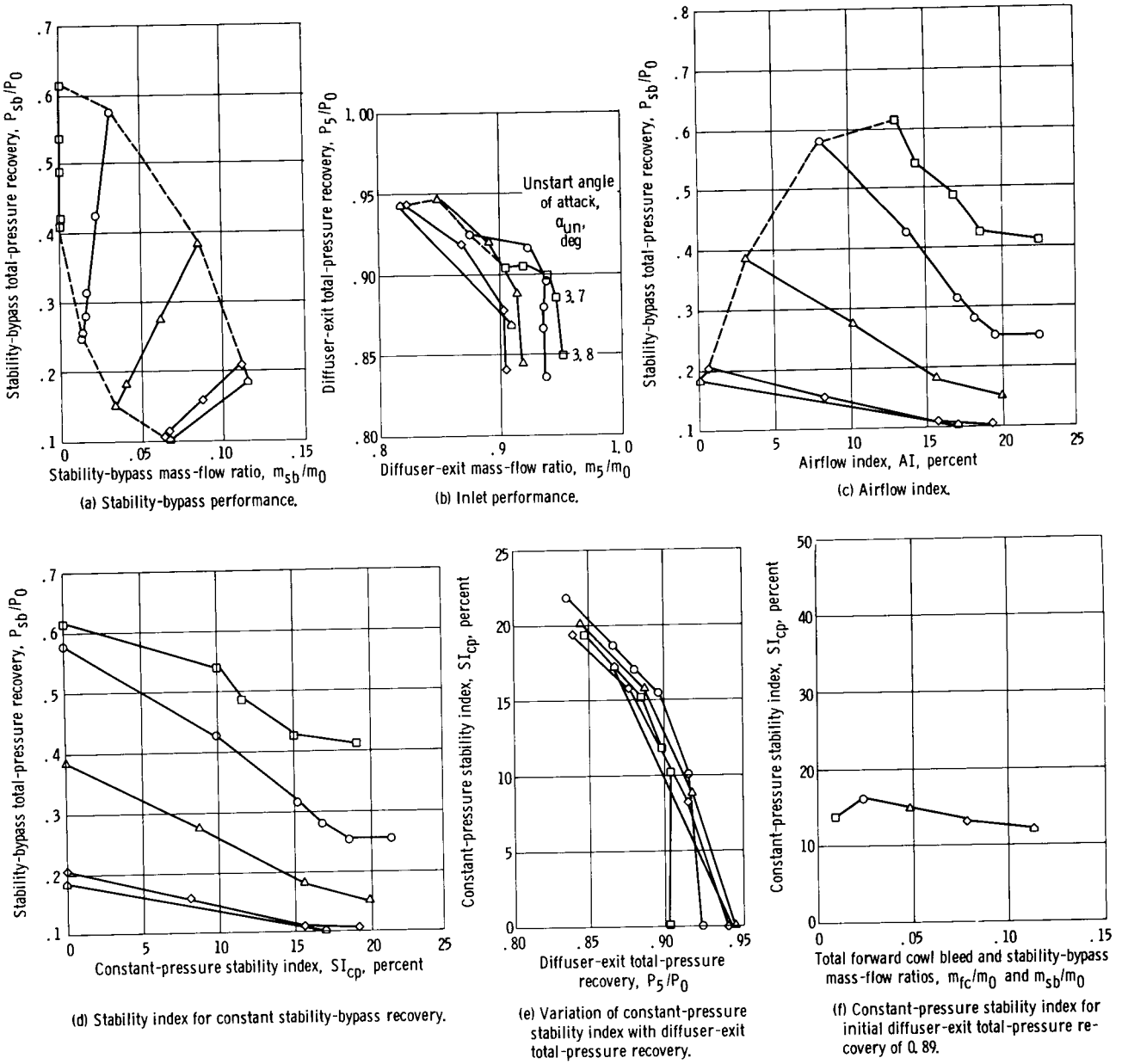

(a) Stability-bypass performance.

(b) Inlet performance.

(c) Airflow index.

(d) Stability index for constant stability-bypass recovery.

(e) Variation of constant-pressure stability index with diffuser-exit total-pressure recovery.

(f) Constant-pressure stability index for initial diffuser-exit total-pressure recovery of 0.89.

Figure 11. - Performance of distributed educated configuration ED. Free-stream Mach number, 2.50; angle of attack, 0°; overboard-bypass mass-flow ratio, 0.01.

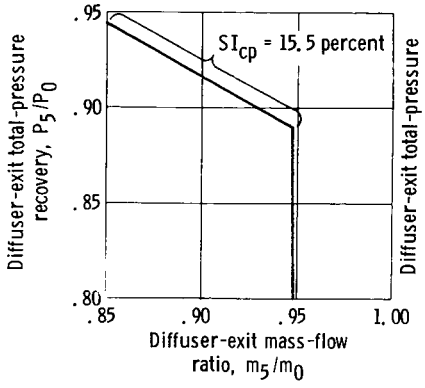

(g) Inlet performance based on constant stability-bypass recovery to unstart limit from initial inlet conditions of 89 percent total-pressure recovery and total forward cowl bleed and stability-bypass mass-flow ratio of 0.02.

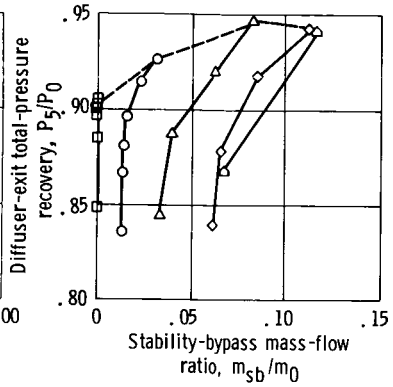

(h) Variation of diffuser-exit total-pressure recovery with stability-bypass mass flow.

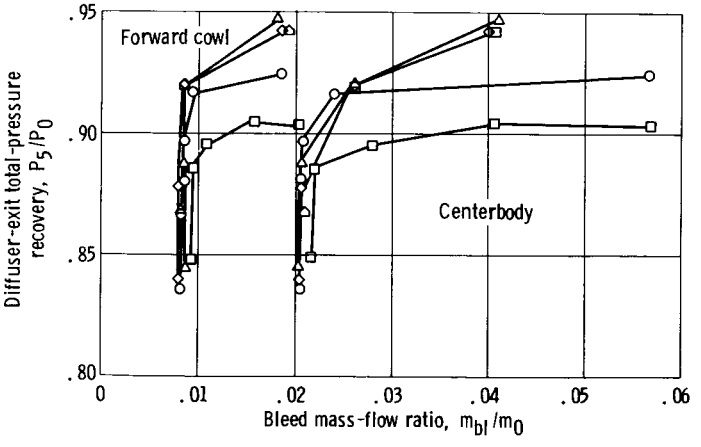

(i) Forward cowl and centerbody bleed performance.

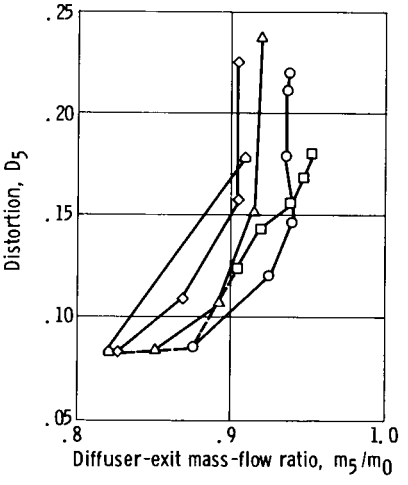

(j) Distortion.

Figure 11. - Concluded.

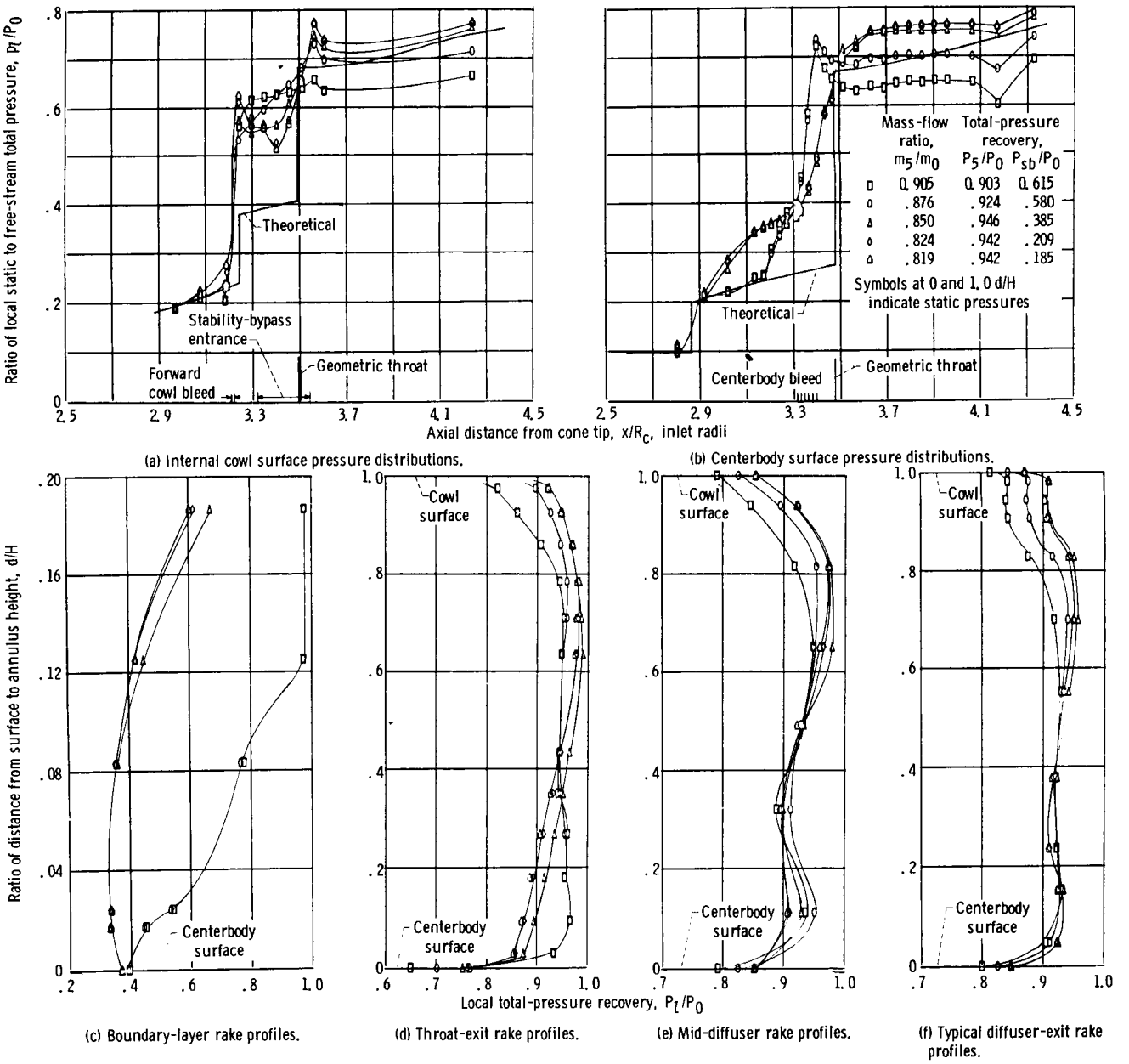

Figure 12 - Diffuser static- and total-pressure distributions for configuration ED at minimum stable operation.

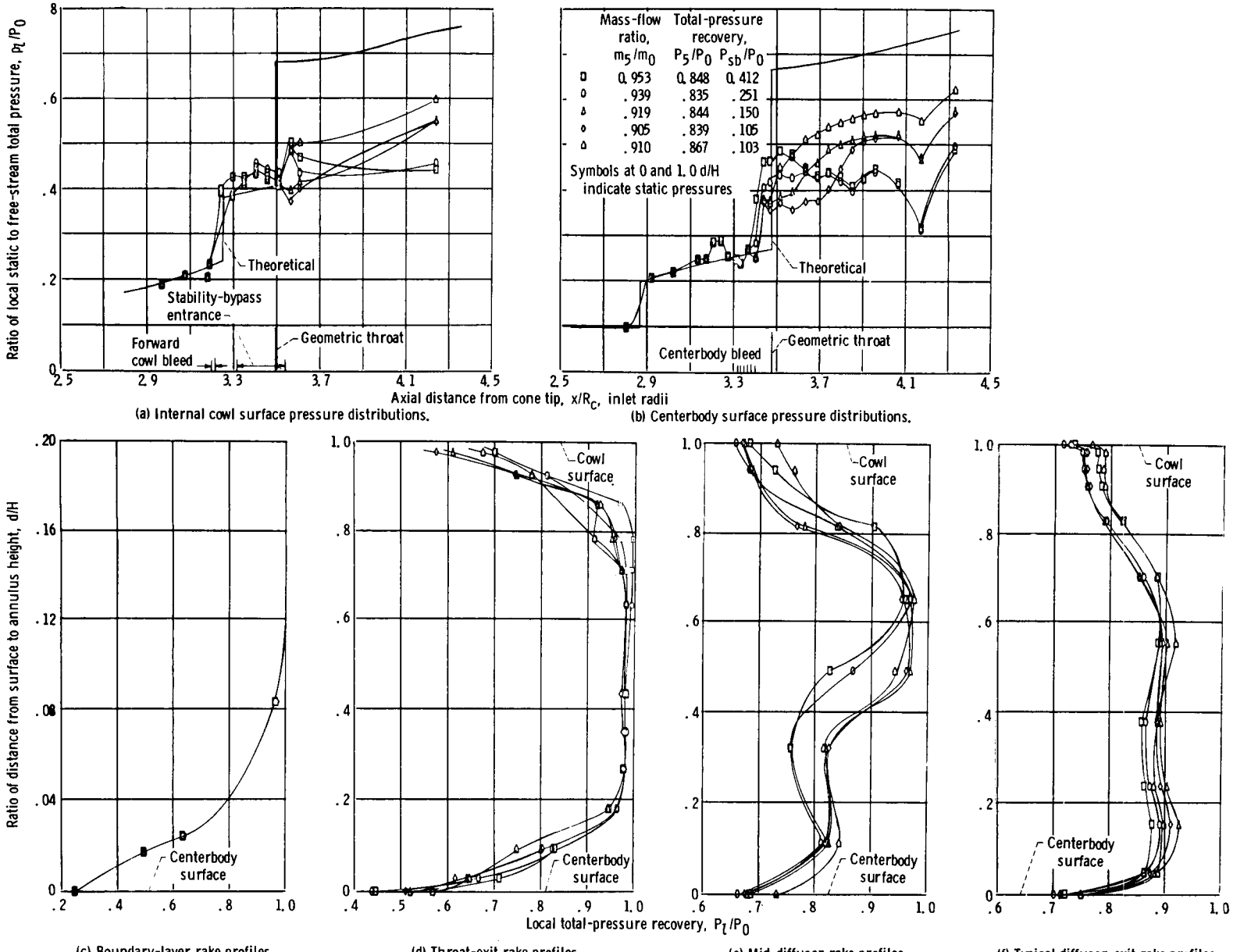

(a) Internal cowl surface pressure distributions.

(b) Centerbody surface pressure distributions.

(c) Boundary-layer rake profiles.

(d) Throat-exit rake profiles.

(e) Mid-diffuser rake profiles.

(f) Typical diffuser-exit rake profiles.

Figure 13. - Diffuser static- and total-pressure distributions for configuration ED at supercritical operation.

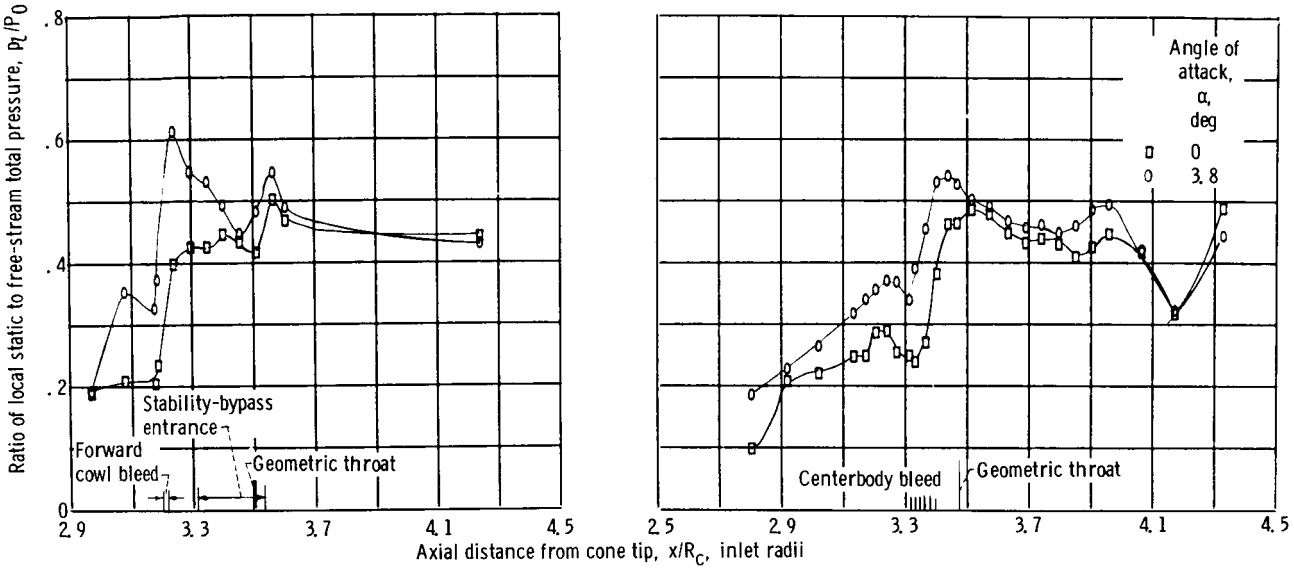

(a) Internal cowl surface pressure distributions.

(b) Centerbody surface pressure distributions.

Figure 14. - Static-pressure distributions at 0^0 angle of attack and maximum angle of attack before unstart (3.8^0).